

Universal lateral distribution of energy deposit in air showers and its application to shower reconstruction

D. Góra,^{a,*} R. Engel,^b D. Heck,^b P. Homola,^a H. Klages,^b
J. Pękala,^a M. Risse,^{a,b} B. Wilczyńska,^a and H. Wilczyński^a

^a *Institute of Nuclear Physics PAN, ul.Radzikowskiego 152,
31-342 Kraków, Poland*

^b *Forschungszentrum Karlsruhe, Institut für Kernphysik, 76021 Karlsruhe,
Germany*

Abstract

The light intensity distribution in a shower image and its implications to the primary energy reconstructed by the fluorescence technique are studied. Based on detailed CORSIKA energy deposit simulations, a universal analytical formula is derived for the lateral distribution of light in the shower image and a correction factor is obtained to account for the fraction of shower light falling into outlying pixels in the detector. The expected light profiles and the corresponding correction of the primary shower energy are illustrated for several typical event geometries. This correction of the shower energy can exceed 10%, depending on shower geometry.

1 Introduction

One of the methods of extensive air shower (EAS) detection is recording fluorescence light emitted by nitrogen molecules in the air along the shower path. For very high energies of the primary particle, enough fluorescence light is produced so that the shower can be recorded from a distance of many kilometers by an appropriate optical detector system [1,2,3]. As the amount of fluorescence light is closely correlated to the ionization energy deposit in air, it provides a calorimetric measure of the primary energy.

* *Correspondence to:* D. Góra (Dariusz.Gora@ifj.edu.pl)

The field of view of a fluorescence detector (FD) telescope is divided into many pixels. For example, in case of the Pierre Auger Observatory (PAO) [4] each pixel views 1.5° of the sky and records the received light in 100 ns time intervals. A shower passing through the telescope field of view triggers some pixels, which form together a "shower track". The lateral width of this track depends on shower geometry but can well be larger than the pixel size.

For a precise energy determination one needs to collect the available signal as completely as possible, i.e. from all detector pixels which receive light from the shower. On the other hand, adding signals from many pixels implies adding the background noise as well. Therefore it is important to include in the analysis only a small number of pixels which contain the "true" shower signal.

In this paper, Monte Carlo simulations of the shower image are presented. Based on the spatial energy deposit of shower particles as calculated by CORSIKA [5,6] it is shown that the lateral shower spread can be well parameterized as a function of the shower age parameter only. The derived parameterization can be used for reconstruction of shower profiles. This is illustrated by applying the new parametrization to the reconstruction of the primary shower energy for several simulated events in a fluorescence detector.

The plan of the paper is the following: the definition of the shower width and algorithm of fluorescence light production based on the CORSIKA simulation of energy deposit density are described in Section 2. In Section 3 an analytical parametrization is derived and its implementation in energy reconstruction procedure is discussed. Conclusions are given in Section 4.

2 Properties of shower image

2.1 Shower width and shape function

Photons which constitute an instantaneous image of the shower originate from a range of shower development stages [7], namely from the surface S shown in Figure 1. These simultaneous photons are defined as those which arrive at the FD during a short time window Δt . During this Δt (corresponding to a small change of the shower position in the sky by $\Delta\chi$) the shower front moves downward along the shower axis by a small distance $\Delta l \simeq R\Delta\chi/\sin(\theta_i)$, where R is the distance from FD to the volume ΔV and θ_i is the angle between the shower axis and the direction towards FD. This means that the small element of surface S corresponds to a small volume ΔV . The number of photons which

arrive to the FD from volume ΔV can be calculated as:

$$dN_{\gamma}^{rec}|_{\Delta V} = f(X, r) dS_{\perp} \times \frac{A}{4\pi R^2} \times \int W(\lambda) \eta(\lambda) d\lambda, \quad (1)$$

where $f(X, r)$ is the distribution of light emitted, dS_{\perp} is the projection of the surface dS onto a surface perpendicular to direction of the shower axis, A is the light collecting area of the detector, $W(\lambda)$ is the light transmission factor, $\eta(\lambda)$ is the normalized fluorescence wavelength spectrum. These photons form an instantaneous image of the shower which can be described by the angular distribution of light recorded by the FD

$$f_{\gamma}(\alpha) \equiv \frac{dN_{\gamma}^{rec}|_{\Delta V}}{\alpha d\alpha d\phi}, \quad (2)$$

where α is the small angle between the direction to the center of the image spot and the direction to volume ΔV , ϕ is the azimuth angle.

The size of shower image is defined as the minimum angular diameter 2α of the image spot containing a certain fraction $F(\alpha)$ of the total light recorded by the FD.

A shower viewed from a large distance has, to a very good approximation, a circular image, independent of the direction of shower axis [2,7]. The intensity distribution of light in this image is proportional to the lateral distribution of the emitted fluorescence light in the shower at the viewed stage of evolution. Therefore the fraction of light received $F(\alpha)$ can be obtained from the corresponding fraction $F(r)$ of light emitted around the shower axis

$$F(\alpha) \equiv \int_0^{\alpha} f_{\gamma}(\alpha') 2\pi \alpha' d\alpha' \sim \int_0^r f(r') 2\pi r' dr' \equiv F(r), \quad (3)$$

where $f(r)$ is the (normalized) lateral distribution of fluorescence light emitted. Here we have neglected the fact that photons from the side of the shower front facing the detector have been emitted at a time later than photons from the farther side of the shower. As will be shown later, relevant lateral distances are in the range 150 to 300 m and hence this is also the distance scale for the maximum time differences of emission [2]. As there is no significant change of the lateral distribution expected of a shower traversing ~ 300 m of air, the effect of different emission is negligible in our calculation.

In the following we shall consider showers close to the FD. For these showers, the optical image size is mainly determined by the geometric size of the shower disk. Light absorption and multiple scattering cause only a minor, negligible modification of the shower image.

The main task is therefore to derive $f(r)$, which is also referred to as the shape function, since the brightness distribution of the shower image depends on the shape of $f(r)$. At the first approximation, the $f(r)$ is proportional to the number of particles in the shower at a given lateral distance, assuming a constant fluorescence yield per particle in the shower. For an electromagnetic shower this number of charged particles is given by the Nishimura-Kamata-Greisen (NKG) function [8]. In this case the $F(r)$ can be determined analytically, as has been shown in Ref. [9]. However, $F(r)$ derived in this way does not describe the light distribution well in case of hadronic showers. This is due to the fact that the number of particles in a hadronic shower does not follow the NKG distribution well.

2.2 CORSIKA approach based on energy deposit density

Although the assumption that the amount of emitted light is proportional to the number of particles is adequate for a determination of the fluorescence signal in many cases, it is here not suited for the following reasons. The fluorescence yield is proportional to the ionization energy deposited by the shower rather than to the total number of charged particles. Furthermore, the simulated number of particles in a Monte Carlo calculation depends on the threshold energies chosen by the user [10,6], above which particles are simulated. Particles falling below the threshold energy are discarded.

A better approximation for the fluorescence yield can be obtained by using the energy deposit $dE(X)/dX$ as a function of atmospheric slant depth interval dX together with a density- and temperature-dependent fluorescence yield $Y(\rho, T)$ [11,12,13]. In this approximation the distribution of photons emitted around the shower axis is proportional to the lateral distribution of energy deposit, $f(r) \sim \frac{dE(X,r)}{dX_v}$, where $dX_v = dX \cos(\theta)$ is the vertical depth interval and θ is the shower zenith angle. The distribution of energy deposit $dE(X)/dX_v$ is calculated with the CORSIKA shower simulation program as the sum of the energy released by charged particles with energies above the simulation threshold plus the releasable energy fraction of particles discarded due to the energy cut. More specifically, the following approximation is used [6]:

$$\frac{dE(X)}{dX_v} = \frac{E_{ioniz}}{\Delta X_v} + \frac{E_{e^\pm, cut}}{\Delta X_v} + \frac{E_{\gamma, cut}}{\Delta X_v} + \frac{1}{3} \frac{E_{\mu^\pm, cut}}{\Delta X_v} + \frac{1}{3} \frac{E_{had, cut}}{\Delta X_v} \quad (4)$$

where E_{ioniz} is the ionization energy deposit of all charged particles traversing the depth interval ΔX_v . $E_{i, cut}$ denotes the energy of particles of type i falling below the simulation threshold within this interval.

In the following we will study the lateral distribution of energy deposit den-

sity in air showers, as it is directly proportional to the number of expected fluorescence photons. Using CORSIKA a two-dimensional energy deposit distribution around the shower axis is stored in histograms during the simulation process for 20 different vertical atmospheric depths. Each of the 20 horizontal layers has a thickness of $\Delta X_v = 1 \text{ g/cm}^2$ and corresponds to a certain atmospheric depth: the first one to $X_1 = 120 \text{ g/cm}^2$ and the last one to $X_{20} = 870 \text{ g/cm}^2$. Linear interpolation between the observation levels is performed in order to get the lateral distribution at a given vertical depth X_n located between two CORSIKA observation levels X_k and X_{k+1} . The fraction of energy deposit $F(r)$ is calculated by numerically integrating the histograms up to the lateral distance r .

The shower simulations are performed with the hadronic interaction models GHEISHA [17] (for interactions below 80 GeV) and QGSJET 01 [18]. Electromagnetic interactions are treated by a customized version of the EGS4 [19,20] code. To reduce computing time, a thinning algorithm [21] is selected within CORSIKA. The thinning level of 10^{-6} has been chosen with the so-called optimum weight limitation [22,23]. This ensures that the artificial fluctuations in the longitudinal shower profiles introduced by the thinning method are sufficiently small for this analysis [10]. The kinetic energy thresholds for explicitly tracking particles were set to: 100, 100, 0.25, 0.25 MeV for hadrons, muons, electrons and photons, respectively.

3 Results

The knowledge of the $F(r)$ function can be used to calculate the "true" signal (light) from shower, which may be divided among several neighboring detector pixels. Below we propose a universal parameterization of $F(r)$ based on CORSIKA simulations and show how the "true" signal can be estimated with this parameterization.

3.1 Fraction of energy deposit density from CORSIKA

In the following we study the dependence of the lateral energy deposit density on various variables.

A natural transverse scale length in air showers, which proves to be useful for obtaining a universal parameterization of the lateral distribution, is given by the Molière radius [15]

$$r_M \equiv E_s \frac{X_l}{\epsilon_0}, \quad (5)$$

where $E_s \simeq 21$ MeV is the scale energy, $\epsilon_0 = 81$ MeV the critical energy and $X_l = 37$ g/cm² the radiation length in air. The local Molière radius at a given atmospheric depth of shower development (at altitude h) can be obtained by dividing Eq. (5) by the air density, $\rho(h)$, and is approximately given by $r_M = 9.6 \text{ gcm}^{-2} / \rho(h)$.

It is also well known that the distribution of particles in a shower at a given depth depends on the history of the changes of r_M along the shower path rather than on the local r_M value at this depth. To take this into account, the r_M value is calculated at 2 cascade units (radiation length X_l) above the considered depth [15]. Using the value of the Molière radius calculated based on the atmospheric profile (the US Standard Atmosphere [16]) for vertical depth $X_n - 2X_l \cos(\theta)$, the fraction of energy deposit density $F(r^*)$ versus the distance in Molière units $r^* = r/r_M$ is found. The knowledge of $F(r^*)$ gives a possibility to study variation of the shape of energy deposit density due to properties of the atmosphere. The variation of the density of the atmosphere along the path of a shower affects the Molière radius and consequently also the radial particle distribution.

To characterize the development stage of a shower, we introduce the shower age parameter

$$s = \frac{3}{1 + 2X_{max}/X}, \quad (6)$$

where X_{max} is the atmospheric depth of shower maximum extracted from simulated data¹. With this definition, a shower reaches its maximum at $s = 1$.

Figure 2 presents the integrals of energy deposit density $F(r)$ and $F(r^*)$ for a vertical proton shower with primary energy $E_0 = 10$ EeV, obtained at different atmospheric depths. It is seen in Figure 2A that the shape of this integral distribution varies considerably only at depths smaller than 360 g/cm². At larger depths, and in particular around the shower maximum, the variation of integral energy deposit profile is not significant. However, this variation is larger when one plots this integral versus distance measured in Molière units, as shown in Figure 2B.

Figure 3A shows the dependence of the integral of energy deposit density $F(r)$ on energy and primary particle. It is seen that the integral profile only slightly depends on energy and primary particle. The differences are even smaller if we plot the fraction of energy deposit density versus distance in Molière units, as shown in Figure 3B. The same shape of the $F(r^*)$ profile for different primaries

¹ X_{max} was determined by fitting a Gaisser-Hillas type function [14] to the CORSIKA longitudinal profile of energy deposit.

and energies means that variations of the $F(r)$ profile are mainly due to the atmospheric effect i.e. dependence of the Molière radius on altitude. For the same shower geometry, there are different altitudes of the maxima of proton and iron showers, and in consequence different values of Molière radius r_M . Since r_M determines the lateral spread of particles in the shower, the shape function $F(r)$ becomes broader for iron showers (higher altitude of shower maximum than for proton shower).

Figure 4 presents the dependence of the integral of energy deposit profile on zenith angle. We note that CORSIKA energy deposit lateral profiles are obtained for horizontal planes at the given observation level, so if one compares energy deposit densities between vertical and inclined showers, a projection of densities from horizontal plane to the plane normal to the shower axis is performed for inclined showers. The corrected profile for a shower inclined at $\theta = 45^\circ$ is shown in Figure 4A by the solid line. It is seen that this profile differs from the profile obtained for a vertical shower. This means that the shape of $F(r)$ depends on the zenith angle. This dependence can be understood if one takes into account the influence of the atmospheric effect on the energy deposit profile $F(r)$. For a homogeneous atmosphere, the shape function for inclined and vertical showers must be the same for the same development stage because the Molière radius does not change with altitude. In case of an inhomogeneous atmosphere, differences of the shape function between vertical and inclined shower should be proportional to the differences of the Molière radius (i.e density of air). Thus if changes of the shape function are due only to the atmospheric effect, then $F(r^*)$ profile should be the same for vertical and inclined showers. Figure 4B confirms this assumption.

The analysis of Figs. 2B, 3B and 4B leads to the following conclusion: *the lateral shape of the energy deposit density versus distance from shower axis measured in Molière units is independent of the primary energy, primary particle type and zenith angle. It depends, to a good approximation, only on the shower age.* Figure 5 confirms this conclusion, too. In this Figure we present the integral of the energy deposit density for different age parameters for 10 individual proton and 5 individual iron showers with different zenith angles ($\theta = 0^\circ, 45^\circ, 60^\circ$) and energy 10 EeV. It is seen that the shower-to-shower fluctuations are strongly reduced for a given age when we correct $F(r)$ profiles for the atmospheric effect i.e. plot $F(r^*)$. Also, there are no differences in the shape of $F(r^*)$ for showers with different zenith angles and primary particle type. This means that it is possible to find a universal function which describes the shape of energy deposit density as a function of shower age only. Following our earlier work [9] we will use the function

$$F(r^*) = 1 - (1 + a(s)r^*)^{-b(s)}, \quad (7)$$

where the parameters $a(s)$ and $b(s)$ are assumed to be functions of shower

age. Fits of this functional form to the integral of energy deposit density were performed for the data from Figures 5B, D, F and are shown in Figure 6. The values of the parameters $a(s)$ and $b(s)$ for different shower ages are presented in Figure 7. The age dependence of $a(s)$ and $b(s)$ parameters is well described by

$$a(s) = 5.151s^4 - 28.925s^3 + 60.056s^2 - 56.718s + 22.331, \quad (8)$$

$$b(s) = -1.039s^2 + 2.251s + 0.676. \quad (9)$$

Thus, Eqs. (7), (8) and (9) give us a universal function which describes the fraction of energy deposit density within a specified distance from the shower axis for different energies, zenith angles and primary particles. Moreover, Eq. (7) can be used to simulate the size of the shower image not only at shower maximum like in Ref. [9], but also for any shower development stage. Inverting Eq. (7) and taking into account the distance from the detector to the shower (R_0) we can find the angular size of the image α that corresponds to a certain fraction of the total fluorescence light signal:

$$\alpha(s) = 2 \arctan \left(\frac{r}{R_0} \right) = 2 \arctan \left(\frac{r_M(s)}{a(s)R_0} ((1 - F(r))^{-1/b(s)} - 1) \right). \quad (10)$$

3.2 Application in energy reconstruction procedure

As the shape of the lateral distribution of energy deposit can be well described by Eq. (7), it may be used to take into account the knowledge on the shower width in the procedure of shower reconstruction in the fluorescence detector.

One of the first steps in shower energy reconstruction is the calculation of the light profile at the aperture of the detector, based on the signal recorded by the detector pixels. This signal is converted to the number of equivalent photons at the detector diaphragm. For example, one procedure to determine such a profile is described in [24]. This algorithm uses as input the reconstructed geometry to locate the shower image on the FD telescope camera in 100 ns intervals. Next, the signal (charge) and noise from pixels lying within a predetermined angular distance $\chi_{S/N}$ from the instantaneous position of the image spot center are collected to find the radius $\chi_{S/N}^{max}$ that maximizes the signal-to-noise ratio **over the whole** shower track. Finally, the charge in each 100 ns time interval (time slot), $L_{S/N}(t)$, within that radius $\chi_{S/N}^{max}$ is found and converted to the number of photons using calibration constants.

This procedure works well for distant showers, when the light collected within the radius $\chi_{S/N}^{max}$ corresponds to about 100% of the true signal, but some differences between the signal within $\chi_{S/N}^{max}$ and the true signal may exist for nearby

showers. In the following we investigate this problem and estimate a correction to the described reconstruction algorithm.

The necessary shower reconstructions were performed using Flores-Eye [25] and FDSim [26] programs. First, FDSim was used to generate events based on the Gaisser-Hillas parameterization. Next, the geometrical and energy reconstruction were performed using Flores-Eye. The reconstructed geometries for some events are listed in Table 1. Using these geometries, we find the collected signal $L_{S/N}(t)$ within angular distance $\chi_{S/N}^{max}$ at each time interval². Then, for the given $\chi_{S/N}^{max}$ the effective radius around shower axis $r_0 = R_0 \tan(\chi_{S/N}^{max})$ and the fraction of light $F(r_0)$ based on the function $F(r)$ was calculated. The fraction $F(r_0)$ for events listed in Table 1 is shown in Figure 8. It is seen that for Event1 $F(r_0)$ changes from 89% for a distance-to-shower $R_0 = 7.0$ km to 87% for $R_0 = 6.0$ km. For other events, the collected fraction of the signal within $\chi_{S/N}^{max}$ increases with increasing distance-to-shower and equals on average about 91%, 94% and 99% for Event2, Event3, Event4, respectively. In other words, some portion of the signal, which falls beyond $\chi_{S/N}^{max}$ is missing in the shower reconstruction procedure. To take into account this lost portion of the signal, the signal $L_{S/N}(t)$ is rescaled according to formula $L_{true}(t) = L_{S/N}(t)/F(r_0)$. In this way, one takes into account the shape of lateral distribution of energy deposit and obtains the new integrated charge $L_{true}(t)$ for each time slot. Thus the part of the signal which was contained in neighboring pixels outside $\chi_{S/N}^{max}$ is accounted for.

It should be pointed out that in general, any reconstruction procedure has to take into account the pixellation of the detector. Independent of the specific approach, the correction procedure developed in this work can be applied. In the following, we demonstrate the influence of this correction on the light profile and on energy determination. In Figure 9A it is shown that our correction leads to considerable differences between the $L_{S/N}(t)$ (dashed line) and $L_{true}(t)$ profile (solid line) for a nearby shower (Event 1). In case of distant showers (like Event4) the profile is almost unchanged (see Figure 9B). It should also be noted that changes in the detector-to-shower distance are accounted for in this approach. A "differential" correction is applied (i.e. for each time slot), which also leads to a better reconstruction of the longitudinal shape (and thus X_{max}) of the shower.

Accepting only a fraction of the signal contained within $\chi_{S/N}^{max}$ directly influences the reconstructed primary energy of the shower. In Table 2 we present the influence of the $L_{S/N}(t)$ correction on the Gaisser-Hillas fit to the reconstructed number of particles in the showers. It is seen that this correction changes both the number of particles at the shower maximum and the position

² The value of $\chi_{S/N}^{max}$ depends on geometry, but for events listed in Table 1 it equals about 1.2°.

of the shower maximum. These changes lead to different estimates of primary energy. In the last column the relative differences $k_E = (E_0^{true} - E_0^{S/N})/E_0^{S/N}$ are listed. One sees that k_E is always positive and decreases from 14% for a distance to shower maximum of $R_0=6.5$ km to 2% for $R_0=23$ km.

4 Conclusions

In this work, the distribution of light in the shower optical image is analyzed, based on the lateral distribution of energy deposited by the shower, as derived from CORSIKA simulations. The lateral distribution of energy deposited is parameterized with a functional form inspired by the NKG distribution. The angular distribution of photons arriving simultaneously at the detector (i.e. the intensity distribution of light in the instantaneous image of the shower) is obtained. The shape of this distribution can be approximated by a universal function that depends on the shower age only.

This universal function is used to derive a correction to the shower energy due to the fraction of light falling into detector pixels located far from the center of the shower image. In the usual procedure of shower reconstruction, signal-to-noise ratio is optimized, so that pixels lying far from the center of the shower image are not included in the analysis. The percentage of shower signal in those outlying pixels was determined in this paper based on the lateral distribution of light in the shower image. The signal recorded by the fluorescence detector in the accepted central pixels is rescaled, so that a corrected light profile of the shower is obtained. For events examined, this correction increases the estimated shower energy by 2–14%, depending on the detector-to-shower distance.

Acknowledgements. This work was partially supported by the Polish Committee for Scientific Research under grants No. PBZ KBN 054/P03/2001 and 2P03B 11024 and in Germany by the DAAD under grant No. PPP 323. MR is supported by the Alexander von Humboldt Foundation.

References

- [1] R.M. Baltrusaitis et al., Nucl. Instr. Meth. **A240** 410 (1985).
- [2] P. Sommers, Astropart. Phys. **3** 349 (1995).
- [3] P. Sommers, C.R. Physique **5** 463 (2004).
- [4] Pierre Auger Collaboration, J. Abraham et al., Nucl. Instr. Meth. **A523** 50 (2004).

- [5] D. Heck et al., Report FZKA 6019, Forschungszentrum Karlsruhe, (1998).
- [6] M. Risse and D. Heck, *Astropart. Phys.* **20** 661 (2004).
- [7] D. Góra et al., *Astropart. Phys.* **16** 129 (2001).
- [8] K. Kamata and J. Nishimura, *Progr. Theor. Phys. Suppl.*, **6** 93 (1958); K. Greisen, *Ann. Rev. Nucl. Sci.* **10** 63 (1960).
- [9] D. Góra et al., *Astropart. Phys.* **22** 29 (2004).
- [10] M. Risse and D. Heck, Pierre Auger Project Note GAP-2002-043.
- [11] F. Kakimoto et al., *Nucl. Instr. Meth.* **A372** 527 (1996).
- [12] M. Nagano et al., *Astropart. Phys.* **20** 293 (2003).
- [13] M. Nagano et al., *Astropart. Phys.* **22** 235 (2004).
- [14] T. Gaisser and A.M. Hillas, *Proc. 15th ICRC, Plovdiv*, **8** 353 (1977).
- [15] K. Greisen, *Prog. Cosmic Ray Phys.* **3** 1 (1956); J.A.J. Matthews, Pierre Auger Project Note GAP-1998-002 (1998).
- [16] National Aeronautics and Space Administration (NASA) U.S. Standard Atmosphere 1976, NASA-TM-X74335 (1976).
- [17] H. Fesefeldt, Report PITHA-85/02, RWTH Aachen (1985).
- [18] N.N. Kalmykov, S.S. Ostapchenko, and A.I. Pavlov, *Nucl. Phys. B (Proc. Suppl.)* **52B** 17 (1997).
- [19] W.R. Nelson, H. Hirayama and D.W.O. Rogers , Report SLAC 265, Stanford Linear Accelerator Center, (1985).
- [20] D. Heck and J. Knapp, Report FZKA 6097, Forschungszentrum Karlsruhe, (1998).
- [21] M. Hillas, *Nucl. Phys. B (Proc. Suppl.)* **52B** 29 (1997).
- [22] M. Kobal et al., *Proc. 26th ICRC, Salt Lake City*, **1** 490 (1999); M. Kobal, *Astropart. Phys.* **15** 259 (2001).
- [23] M. Risse et al., *Proc. 27th ICRC, Hamburg*, **2** 522 (2001).
- [24] B. Dawson, Pierre Auger Project Note GAP-2001-016.
- [25] Flores-Eye program distribution web page at Milano:
http://topserver.mi.infn.it/auger/software_development.htm.
- [26] L. Prado et al., submitted to *Nucl. Instr. Meth. A* (2004).

Table 1

Characteristics of events used for the comparisons in this paper. The shower zenith angle θ , azimuth angle ϕ , core position X_c , Y_c are measured relative to FD detector.

Event	θ (deg)	ϕ (deg)	X_c (km)	Y_c (km)
Event1	0.	-15	-0.820	5.860
Event2	60	175	4.535	6.906
Event3	45	20	2.282	7.066
Event4	45	50	-7.665	19.11

Table 2

Comparison of Gaisser-Hillas function parameters based on the $L_{true}(t)$ and the $L_{S/N}(t)$ light profiles and their influence on primary energy. The number of particles at shower maximum N_{max} , corresponding slant depth X_{max} , estimated energy E_0 and relative difference $k_E = (E_0^{true} - E_0^{S/N})/E_0^{S/N}$ are listed as a function of distance R_0 from detector to shower maximum. Calculations are made using the function $F(r^*)$ described by Eq. (7).

Event	R_0 (km)	$N_{max}^{S/N}$ (10^9)	N_{max}^{true} (10^9)	$X_{max}^{S/N}$ (g/cm^2)	X_{max}^{true} (g/cm^2)	$E_0^{S/N}$ (EeV)	E_0^{true} (EeV)	k_E (%)
Event1	6.4	0.93	1.06	701	706	1.370	1.562	14
Event2	8	6.57	6.88	759	767	9.853	10.40	6
Event3	11	2.12	2.19	637	642	2.950	3.100	5
Event4	23	12.85	13.10	752	753	19.20	19.57	2

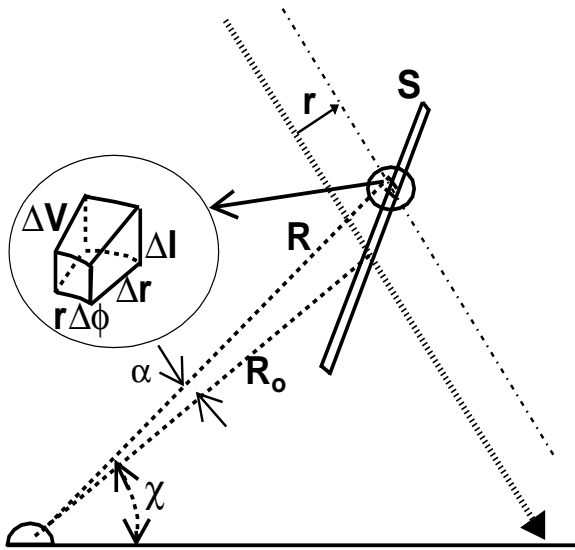


Fig. 1. Geometry of an EAS as seen by the fluorescence detector. Photons which arrive simultaneously at the FD originate from the surface S . See text for more details.

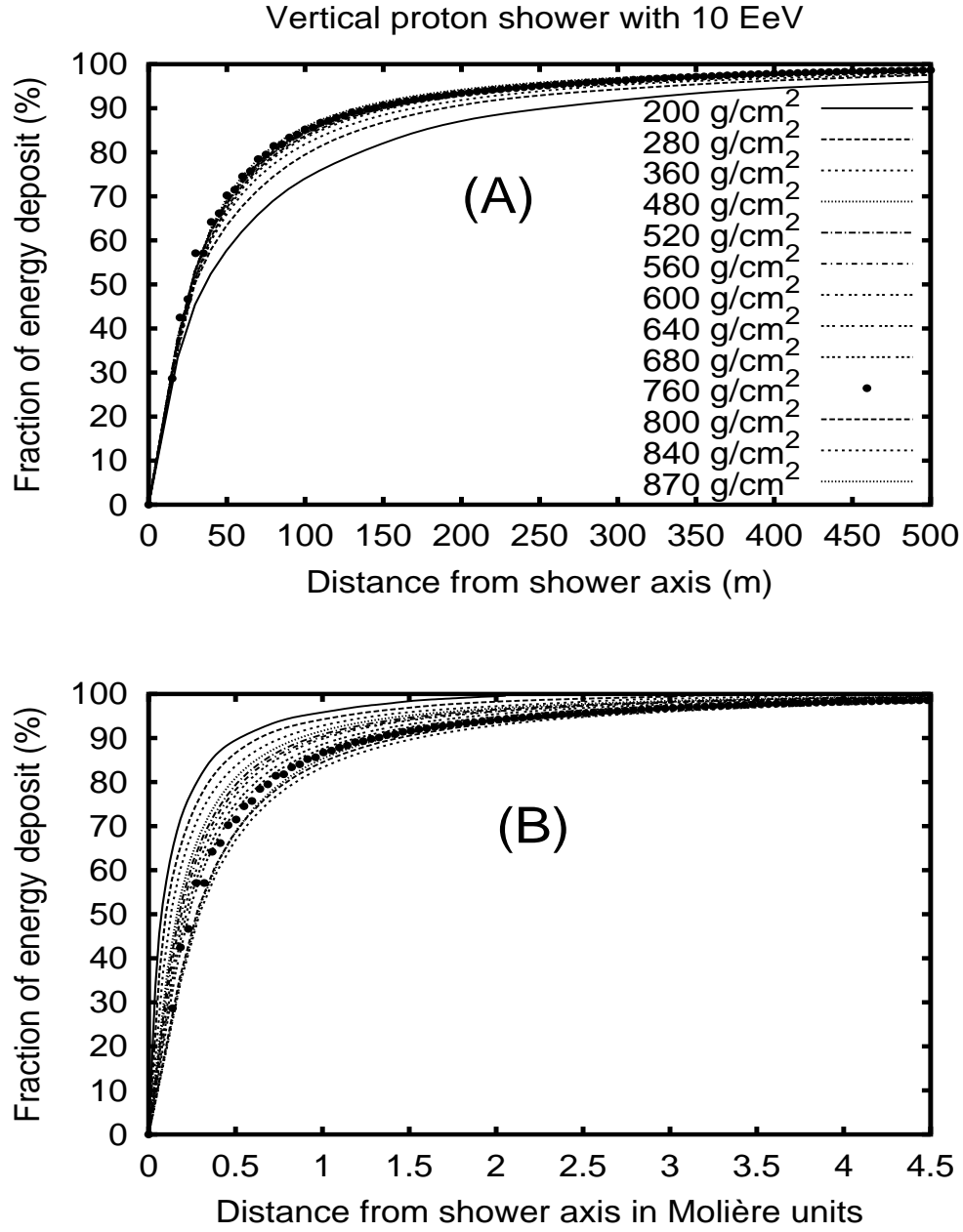


Fig. 2. (A) Integral of energy deposit density $F(r)$ versus distance from shower axis for proton shower; (B) Integral of energy deposit density $F(r^*)$ versus distance from shower axis measured in the Molière units. Different lines described in the top panel correspond to profiles obtained for different vertical atmospheric depths. The profile corresponding to shower maximum is marked by dots.

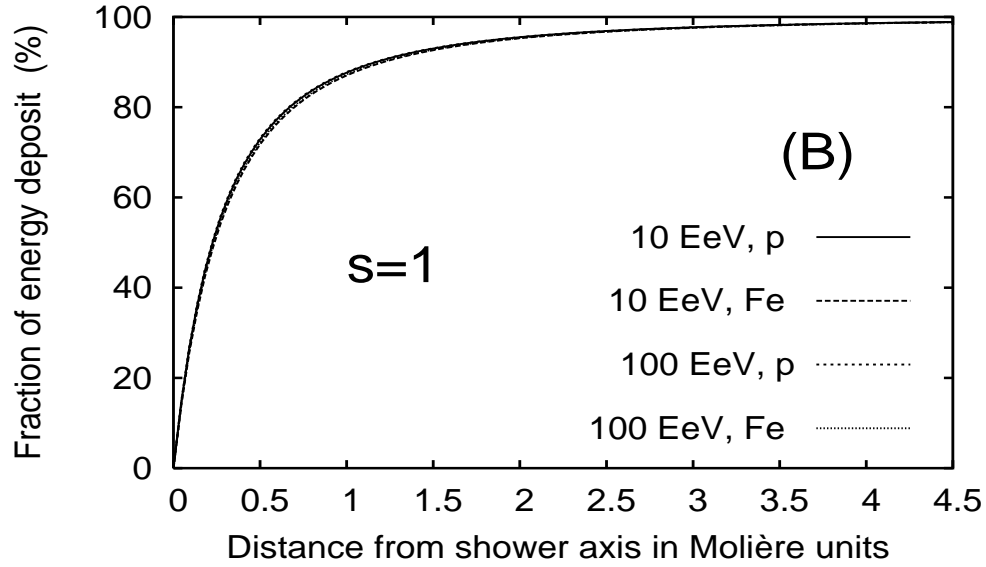
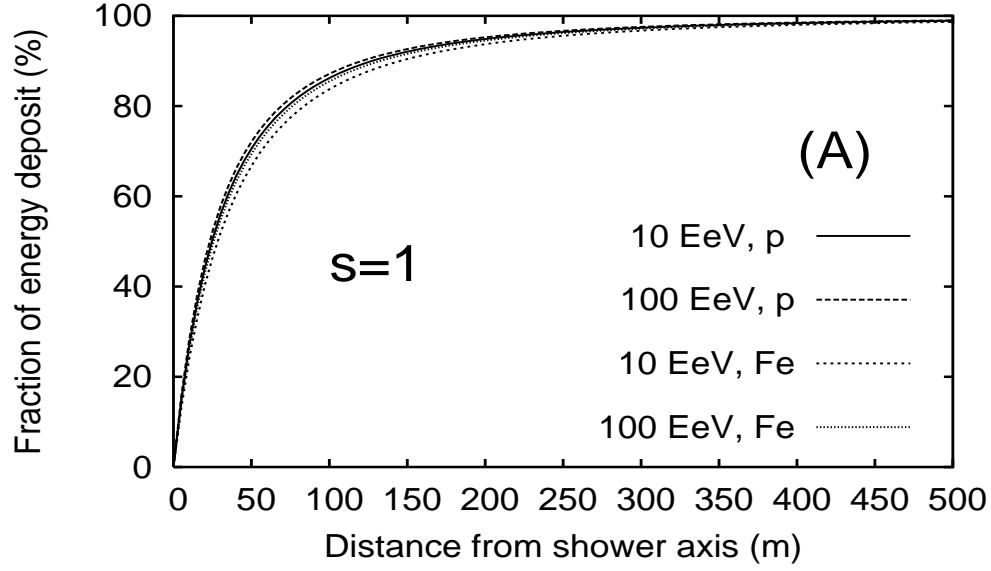


Fig. 3. (A) Integral of energy deposit density versus distance from shower axis; (B) The integral profiles versus distance measured in Molière units; The profiles are shown for vertical showers (at $s=1$) with different primary particle type and energy.

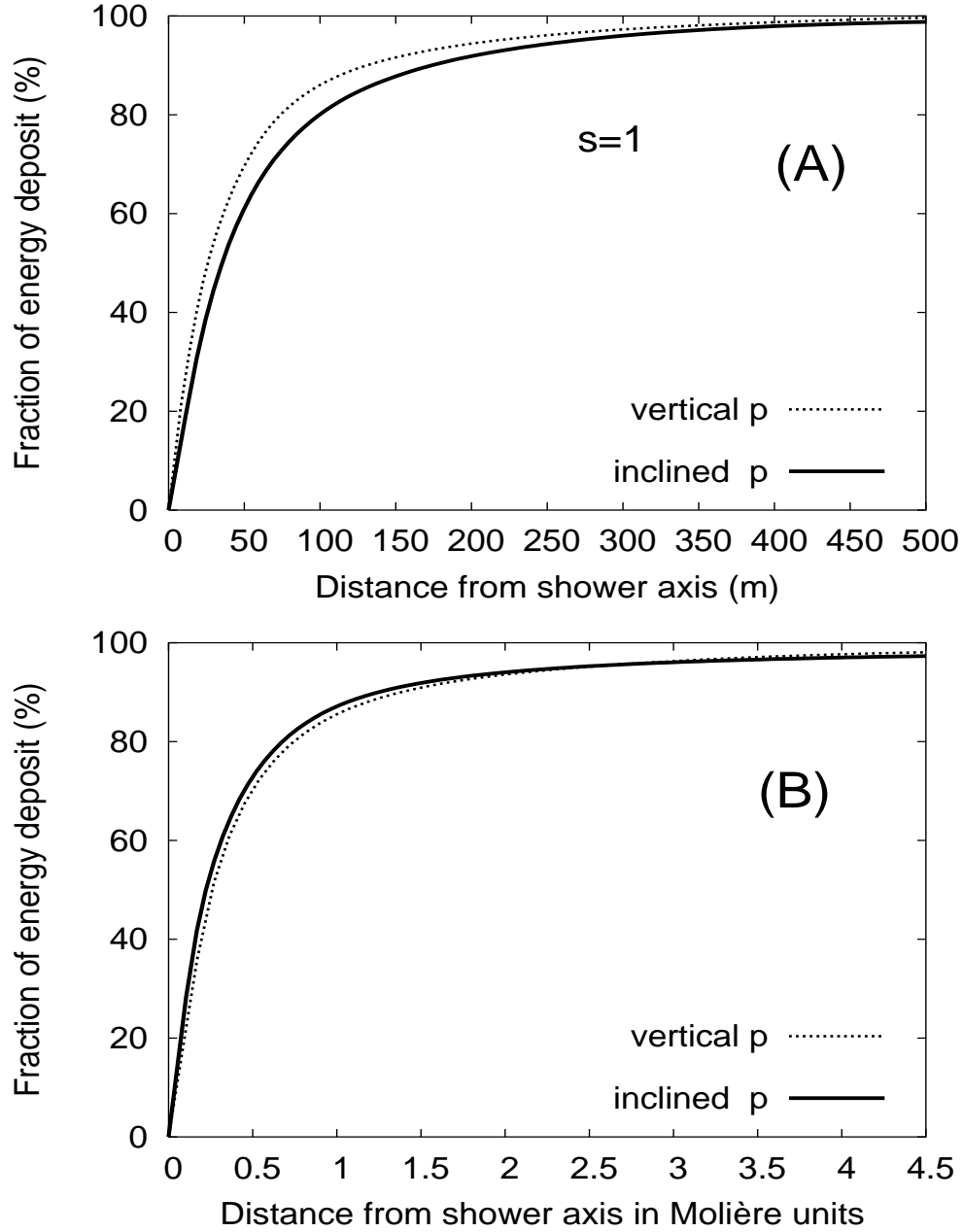


Fig. 4. (A) Integral of energy deposit density versus distance from shower axis for vertical and inclined ($\theta = 45^\circ$) proton showers; (B) The integral profile measured in Molière units. The profiles are shown for 10 EeV showers at $s = 1$.

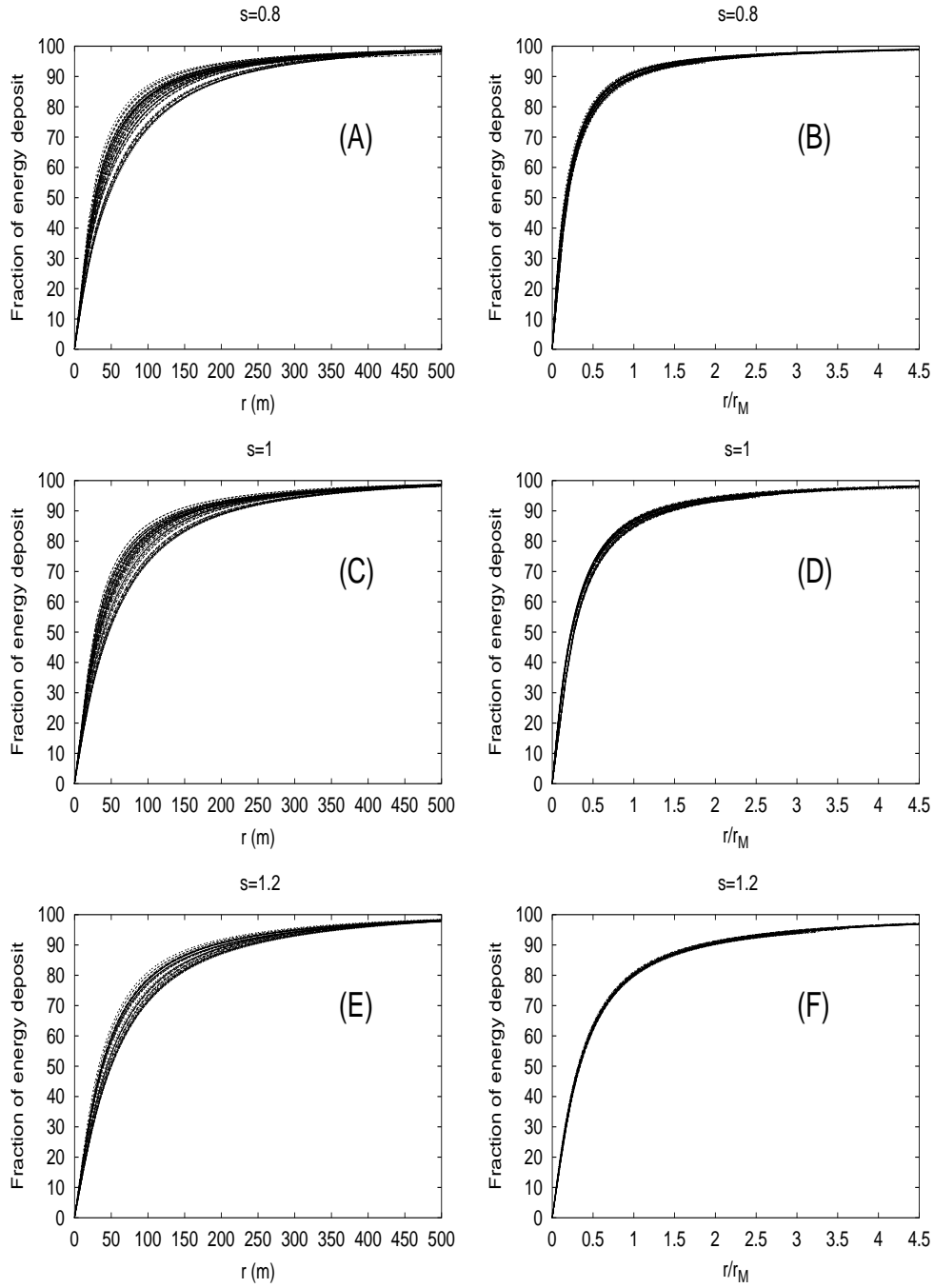


Fig. 5. (A), (C), (E) Integral of energy deposit density versus distance from shower axis; (B), (D), (F) Integral of energy deposit density versus distance measured in Molière units. Individual profiles are obtained for showers with different age, zenith angle and primary particles.

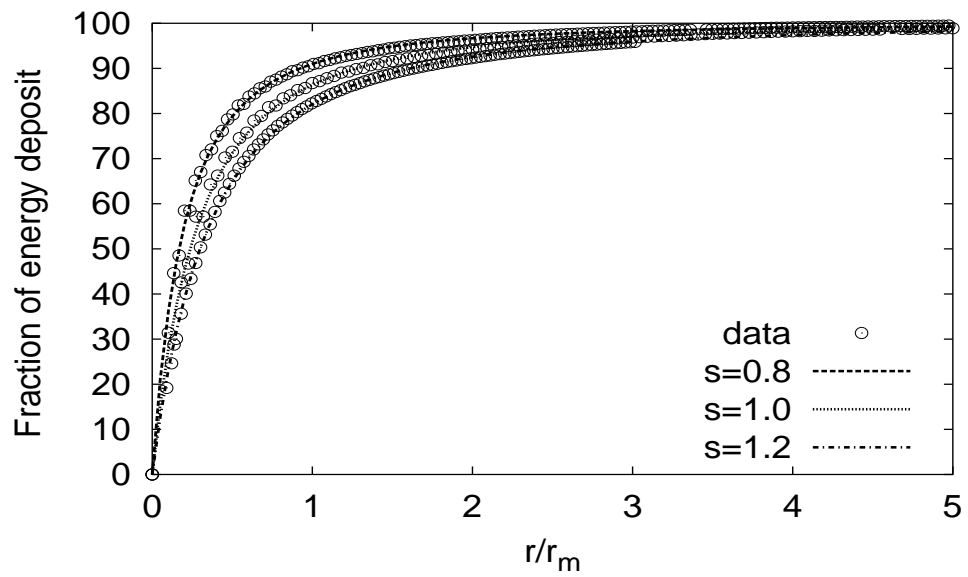


Fig. 6. The fit of function Eq. (7) to fraction of energy deposit density from Figure 5B, D, F for different values of the age parameter s .

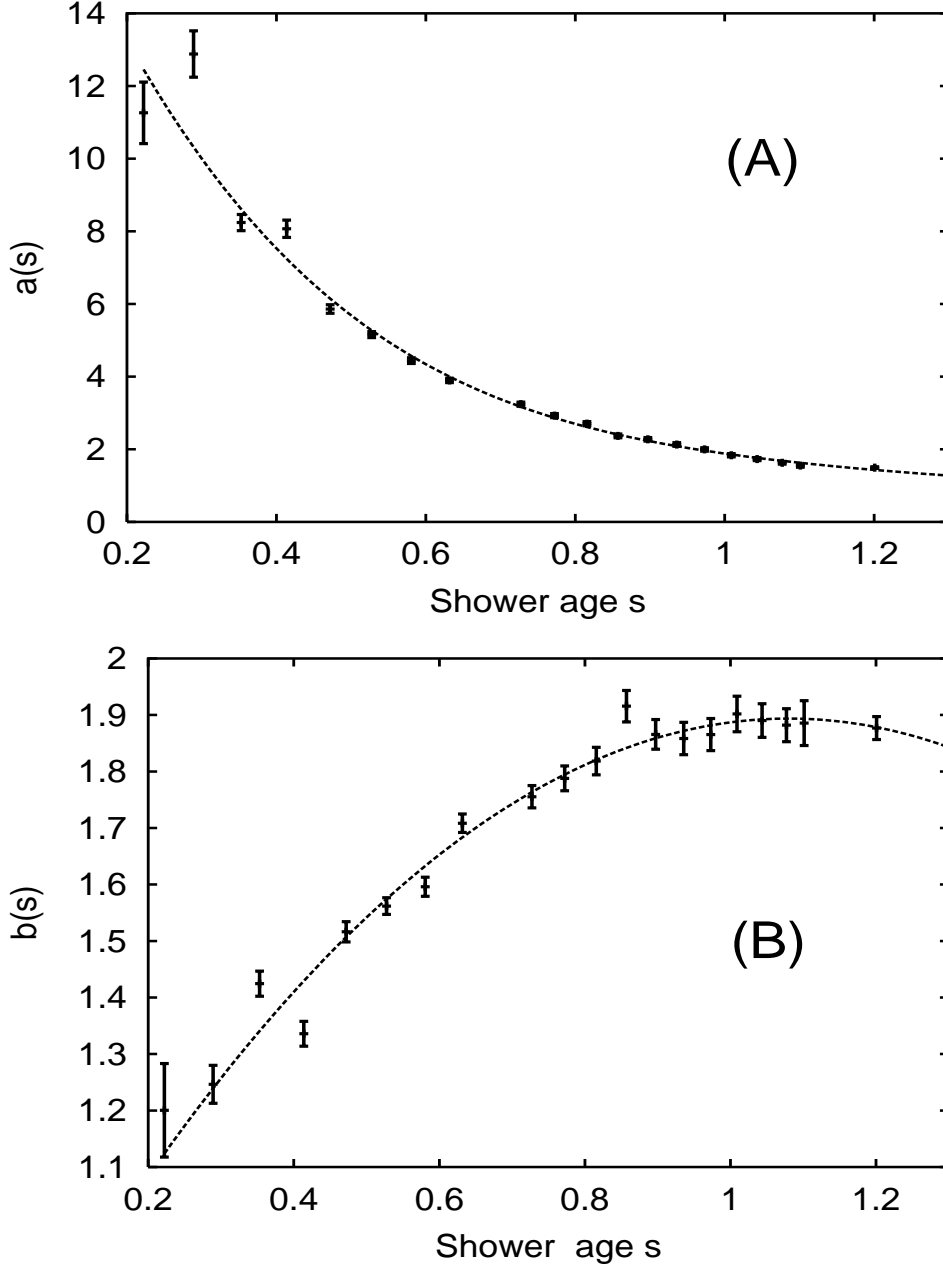


Fig. 7. Values of parameters $a(s)$ and $b(s)$ of Eqs. (8) and (9) obtained based on integral of CORSIKA energy deposit density for vertical showers at energy 10 EeV.

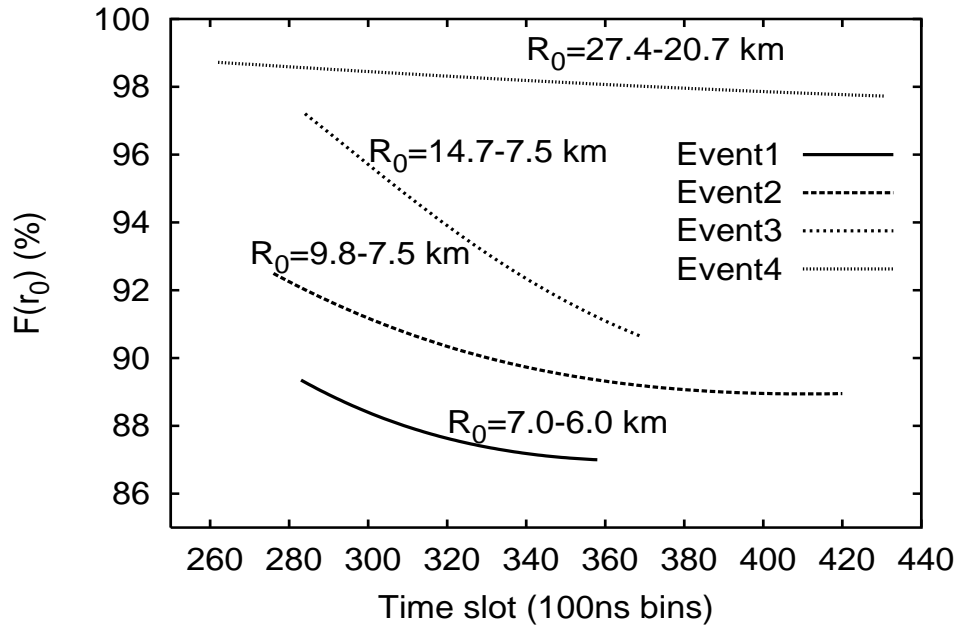


Fig. 8. Fraction of light collected within the angle $\chi_{S/N}^{max}$ versus time for some simulated events. See text for more details.

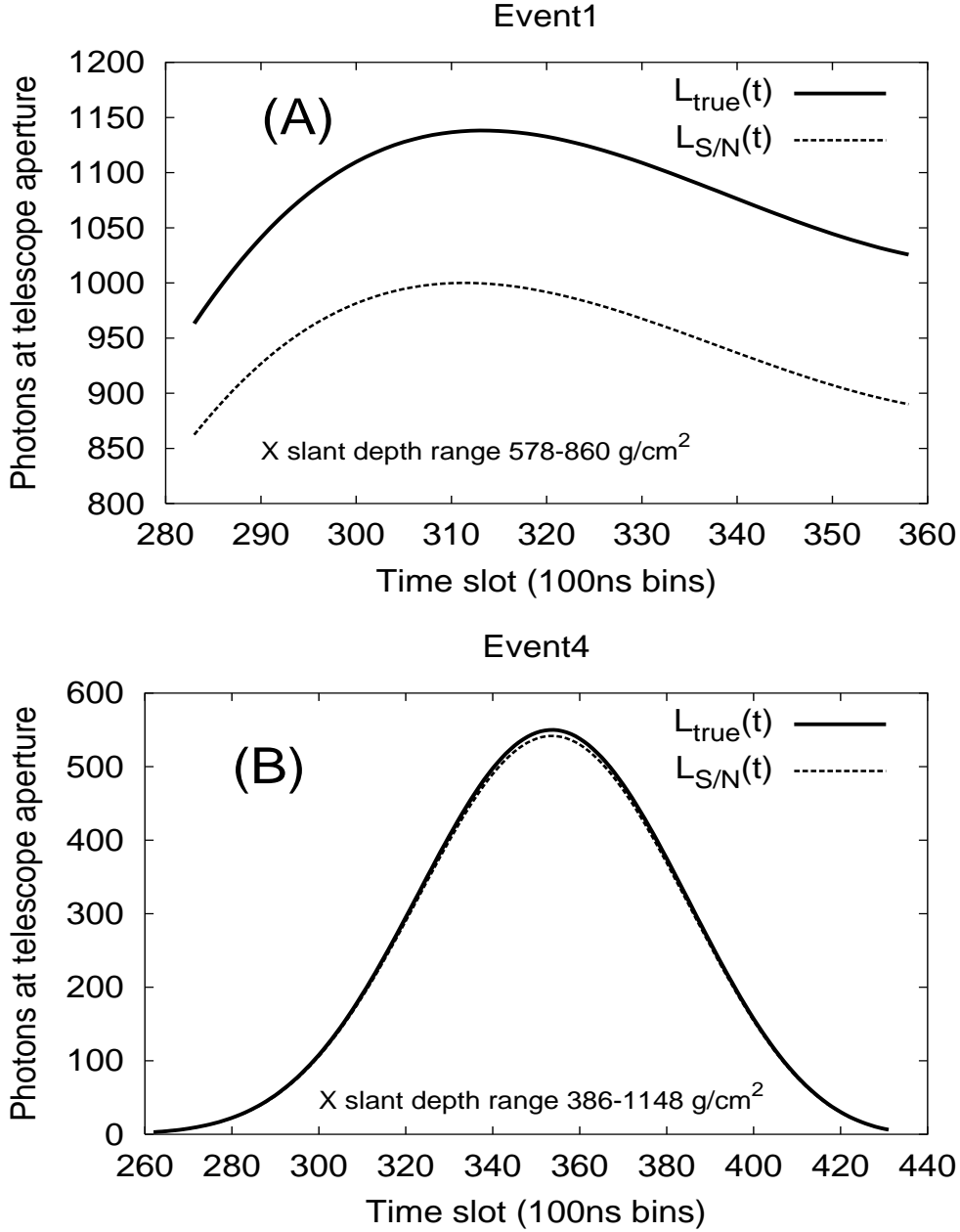


Fig. 9. (A) Comparison of light profiles versus time slot number for Event1. The $L_{S/N}(t)$ light profile (dashed line) is obtained based on the signal-to-noise algorithm implemented in FloresEye. The $L_{true}(t)$ light profile (solid line) is obtained using the shape of $F(r)$ function derived from Eq. (7). (B) Comparison of light profile versus time slot number for Event4.